Biophysical Chemistry 7 (1977) 103–114
© North-Holland Publishing Company

ISOELECTRIC FOCUSING OF INTERACTING SYSTEMS. I. CARRIER AMPHOLYTE-INDUCED MACROMOLECULAR ISOMERIZATION*

John R. CANN and Donald I. STIMPSON
Department of Biophysics and Genetics, University of Colorado Medical Center, Denver, Colorado 80262, USA

Received 10 March 1977

A phenomenological theory of isoelectric focusing is formulated for rapidly reversible, ampholyte-induced macromolecular isomerization. The calculations reveal that such interactions can give well resolved, bimodal transient and equilibrium isoelectric focusing patterns in which the two peaks correspond to different chemical equilibrium compositions and not to separated isomers. The kinetics of approach to the equilibrium pattern are characteristically biphasic: During the first phase, which is controlled by the rate of migration of the isomers in the electric field, two peaks are positioned in the region between the isoelectric points of the two isomers; one of the peaks then grows slowly at the expense of the other with a diffusion-dominated rate. The kinetics are dependent upon the initial distribution of macromolecule in the isoelectric focusing column, and in certain cases only a single peak is apparent during the first phase. These findings have practical implications for unambiguous interpretation of isoelectric focusing patterns, furnish explanations for hitherto puzzling experimental observations, and provide theoretical insights required for application of isoelectric focusing to the detection and characterization of macromolecular interactions in general.

1. Introduction

Isoelectric focusing in natural pH gradients [1–7] is finding wide application to the separation and characterization of proteins and other amphoteric macromolecules with respect to isoelectric point (pI) The method can be described as follows: A linear pH gradient is generated and maintained by electrolysis of carrier ampholytes, each initially distributed uniformly, in a liquid column using a sucrose density gradient to stabilize the system against convective disturbances or in a column or slab of solid support such as polyacrylamide gel. (The commonly used carrier ampholytes are mixtures of relatively small aliphatic polyamino–polycarboxylic acids with high conductances and closely spaced pI's supplied by LKB, Stockholm, Sweden, under the trade name "Ampholine".) During electrolysis the most acidic ampholyte migrates to the anode where it accumulates in its isoelectric state and, due to its buffering capacity, confers upon the immediate environment a pH corresponding to its pI. Simultaneously, the ampholyte with second lowest pI converges from both ends of the column to accumulate in a zone just behind the first ampholyte where it dictates a pH equal to its pI, and so on for the others in the mixture. When the steady state is reached the various carrier ampholytes are distributed along the column from anode to cathode in order of increasing pI; thus, the generated pH gradient. The several zones of ampholyte are not completely separated one from another, however, but overlap to some extent due to coupling through the conductance. Nevertheless, to the first approximation the concentration of each can be considered as being distributed in a gaussian fashion about its pI with a variance dependent upon (1) its diffusion coefficient; (2) the electric field strength maintained by the current carried by the cations and anions of the several ampholytes; and (3) the gradient of electro-

* Supported in part by Research Grant 5R01 HL13909-25 from the National Heart and Lung Institute, National Institutes of Health, United States Public Health Service. This publication is No. 666 from the Department of Biophysics and Genetics, University of Colorado Medical Center, Denver, Colorado 80262.

phoretic mobility of the particular ampholyte which, in turn, is determined by both the dependence of mobility upon pH and the pH gradient. When a zone of isoelectrically homogeneous protein is inserted into the pH gradient at some arbitrary position, the protein molecules migrate under the influence of the electric field toward either the anode or the cathode depending upon the pH ($\neq$pI) at the point of insertion until they reach that position in the column where the pH corresponds to the pI. The protein focuses sharlpy at this position with a concentration distribution governed by the same molecular and environmental factors as in the case of a carrier ampholyte. If the protein is isoelectrically heterogeneous, each of the components focuses at its respective pI so that the isoelectric focusing pattern (plot of concentration versus position) shows a corresponding number of peaks.

The foregoing experimental procedure is commonly used for isoelectric focusing in gels. Alternatively, the carrier ampholytes and the sample of protein can be premixed so that initially both are uniformly distributed throughout the gel or liquid column. Upon establishing the electric field the pH gradient is generated relatively rapidly because of the high mobilities of the ampholytes, after which each protein component converges upon the point in the pH gradient corresponding to its pI. With either procedure the whole process may be completed in a time as short as 5 h or as long as 3–4 days determined by instrumental design, adjustable parameters and electrophoretic properties of the protein. The distribution of protein in the final isoelectric focusing pattern is an equilibrium distribution given the particular environment created by the steady state distribution of carrier ampholytes.

The described behavior is for ideal situations uncomplicated by macromolecular interactions. One might expect rather different isoelectric focusing patterns unamenable to classical interpretation for systems undergoing reversible carrier ampholyte-induced macromolecular isomerization, association or dissociation into subunits, and reversible pH-dependent conformational transitions. In all of these cases the pK of one or more ionizable groups may be altered due to change in conformation or state of association, thereby leading to a change in pI. A few such systems have been investigated; for example, either ampholyte-induced or pH-dependent conformational transition of tRNA [8] and the pH-dependent conformational transition of the 12S subunit protein of the capsid of foot-and-mouth disease virus [9]. Several other systems reported in the literature suggest such interactions [10–12]. Accordingly, theoretical isoelectric focusing patterns have been calculated for several model systems; the results will be reported in a series of papers. In this, the first of the series, we describe the results for the ampholyte-induced isomerization reaction

$$\mathcal{M} + n\mathcal{A} \rightleftharpoons \mathcal{N}\mathcal{A}_n , \qquad (I)$$

where $\mathcal{M}$ is an amphoteric macromolecule, and $\mathcal{A}$ is a carrier ampholyte molecule of which a fixed number, n, are bound into the complex $\mathcal{N}\mathcal{A}_n$, in which $\mathcal{N}$ is an isomer with different electrophoretic mobilities at the same pH-values and a different pI than $\mathcal{M}$. Assignment of different electrophoretic properties to $\mathcal{M}$ and $\mathcal{N}$ is the salient feature of the model, since reversible binding of ampholyte by the macromolecule without concomitant isomerization would have little consequence for isoelectric focusing. As pointed out by Vesterberg and Svenssen [3] a focused macromolecule is in a medium of ampholytes which are essentially isoelectric, so that any ampholyte-macromolecule complexes with the same conformation as the uncomplexed macromolecule would have virtually the same pI.

Since the pI's of $\mathcal{M}$ and $\mathcal{N}$ differ, it is evident that hydrogen ion must be involved in the isomerization reaction. Consequently, the "equilibrium constant" for reaction (I) must incorporate the pK's of the isomers in such a way as to be a function of hydrogen ion concentration. We shall assume that the "equilibrium constant" is an insensitive function of pH and can be considered constant in the region of the column where the system focuses, given the shallow pH gradient and the relatively small difference in pI's.

2. Theory

The theory to be described is for both the equilibrium distribution of macromolecule along the isoelectric focusing column and the time-course of approach to that distribution. Let us first consider the approach to equilibrium.

Most of the calculations simulate the experimental procedure in which the steady state distribution of carrier ampholytes along the column and, thus, the pH gradient are established before inserting a narrow zone of macromolecule into the column. The others are for a broad initial zone. These can be placed into correspondence with the alternative experimental procedure, in which both the macromolecule and the ampholytes are distributed uniformly throughout the column initially, by making the limiting assumption that the steady state is established so rapidly that, in effect, it obtains at the instant the macromolecule begins to migrate under the influence of the electric field. In both cases, it is assumed that the concentration of ampholyte(s) is sufficiently greater than the concentration of macromolecule that it is not perturbed significantly by reaction with the macromolecule. Thus, both the distribution of ampholyte(s) and the pH gradient are invariant in time.

Theoretical time-dependent profiles of macromolecule concentration versus position along the electrofocusing column were computed by numerical solution of the transport equation for constituent macromolecule *. The computations are for the limiting case of rates of reaction so fast that, in effect, there is local chemical equilibrium among the interacting species. Imagine the column to be divided into a number of discrete segments so that the dependent variables become the average concentrations of the two macromolecular species in each segment with driven velocities specified at the interfaces between segments. The average concentration of ampholyte in each segment is also specified. Then, given the initial concentration of the two macromolecular species at chemical equilibrium in each segment, we calculate the change in the distribution of material during a short interval of time, Δt, due to diffusion and driven transport. It is assumed that there is no reequilibration by chemical reaction during Δt, each species migrating independently from its distribution at the beginning of the interval. After the concentrations have been advanced, chemical equilibrium is recalculated. That is, for known constituent concentrations of macromolecule computed from the concentrations of the two species as changed by the transport processes, new equilibrium concentrations are calculated by applying the law of mass action. We then compute the change in this new distribution of material due to transport over the next Δt; recalculate the chemical equilibrium; and so on, thereby constructing the approach to the equilibrium distribution; i.e., the equilibrium isoelectric focusing pattern in contradistinction to the transient patterns which pertain to the approach.

The equilibrium isoelectric focusing pattern itself was calculated by (1) substituting the mass action expression into the transport equation for constituent macromolecule to give the equation of continuity which conserves total macromolecule by taking into account diffusion, driven transport and chemical reaction; (2) equating both the change in concentration with time and the net flow of material to zero; and (3) integrating the resulting ordinary differential equation numerically.

The numerical procedures are outlines below in a format which first considers control calculations on a mixture of two noninteracting macromolecules with different pI's and on a single macromolecule undergoing the simple isomerization reaction

$$\mathcal{M} \rightleftharpoons \mathcal{N} \qquad \text{(II)}$$

and then proceeds to the ampholyte-induced isomerization reaction (I). As in the case of reaction (I) it is assumed that the "equilibrium constant" for reaction (II) is an insensitive function of pH and, thus, can be approximated by a constant.

2.1. Two noninteracting macromolecules

The changes in concentration of the two macromolecules with time, t, and position in the isoelectric focusing column, x, during their independent approach to equilibrium are described by the transport equations

$$\frac{\partial C_k(x,t)}{\partial t} = \frac{\partial}{\partial x}\left[D_k \frac{\partial C_k(x,t)}{\partial x} - V_k(x) C_k(x,t)\right], \quad k = 1, 2, \qquad \text{(I)}$$

where the subscript $k = 1$ designates the macromolecule with higher pI; $C_k(x, t)$ is the molar concentration;

* The equation is for ideal transport in a uniform electric field and neglects hydrodynamic effects of macromolecule concentration and sucrose density and viscosity gradients upon diffusion coefficients and electrophoretic mobilities; possible geometrical effects of gel structure such as molecular sieving; electro-osmosis, etc.

D_k is the diffusion coefficient; and $V_k(x)$ is the driven velocity. $V_k = \mu_k(x)E$ in which $\mu_k(x)$ is the electrophoretic mobility and E, the electric field strength. It is assumed that the electrophoretic mobilities vary linearly with pH as is typical of proteins in the region of their pI's and that $\mathrm{pH}(x) = \alpha + \beta x$. Thus, $V_k(x) = a_k - b_k x$.

We now divide the column into J discrete segments using $J+1$ equally spaced interfaces positioned at $x_j = j\Delta x$ ($j = 0, 1 \ldots J$), introduce the discrete time variable $t_n = n\Delta t$ ($n = 0, 1, 2 \ldots$), and adopt the notation $\bar{C}_k(j, t_n)$ for the average concentration in the segment bounded by x_{j-1}, x_j at time t_n and $V_k(x_j)$ for the driven velocity at interface j. The gradients of driven velocity are positioned such that each pI is centered in a segment; i.e., $V_k(x_j) \neq 0$. Applying the mathematical analysis of Goad [13] as it pertains to the method of first differences, eqs. (1) are approximated by the explicit finite difference equations

$$\bar{C}_k(j, t_{n+1}) = \bar{C}_k(j, t_n) + (\Delta t/\Delta x)(J_{D,k} - J_{E,k}), \quad (2)$$

in which the diffusional flow $J_{D,k}$ is given by

$$J_{D,k} = (1/\Delta x)\{[D_k - |V_k(x_j)|\Delta x/2] \times [\bar{C}_k(j+1, t_n) - \bar{C}_k(j, t_n)] - [D_k - |V_k(x_{j-1})|\Delta x/2] \times [\bar{C}_k(j, t_n) - \bar{C}_k(j-1, t_n)]\} \quad (3)$$

and the driven flow $J_{E,k} = [\delta V_k C_k]_{\mathrm{for}}$ where

$$[\delta V_k C_k]_{\mathrm{for}} = V_k(x_j)\bar{C}_k(j, t_n) - V_k(x_{j-1})\bar{C}_k(j-1, t_n),$$

$$\text{for } V(x_{j-1}),\ V(x_j) > 0;$$

$$= V_k(x_j)\bar{C}_k(j+1, t_n) - V_k(x_{j-1})\bar{C}_k(j, t_n),$$

$$\text{for } V(x_{j-1}),\ V(x_j) < 0;$$

$$= V_k(x_j)\bar{C}_k(j+1, t_n) - V(x_{j-1})\bar{C}_k(j-1, t_n),$$

$$\text{for } V(x_{j-1}) > 0,\ V(x_j) < 0. \quad (4)$$

In eq. (3) the terms $|V_k|\Delta x/2$ compensates for the major fraction of the truncation error due to the way the first spatial derivative is approximated at each interface [13–15], the remaining error $O[(\Delta x)^2]$ being made appropriately small by choosing Δx sufficiently small.

Given values of $\bar{C}_k$ at any time t, we can calculate their values at $t + \Delta t$ as changed by transport using eqs. (2)–(4), the new values serving as the starting distribution of material for the next time cycle of transport, and so on. Thus, given initial conditions and boundary values, this recursive calculation allows one to follow the approach to equilibrium. The initial conditions are $\bar{C}_k(j, 0) = \bar{C}_k^0$ for $j = j', \ldots j' + J'$ and $\bar{C}_k(j, 0) = 0$ for $j \neq j', \ldots j' + J'$. The boundary values are $\bar{C}_k(1, t_n) = \bar{C}_k(J, t_n) = 0$.

Error estimates on the numerical solution of eqs. (1) are provided by the analytical relationships

$$\bar{x}_k(t) = a_k/b_k + [\bar{x}_k(0) - a_k/b_k]\exp(-b_k t) \quad (5)$$

and

$$\sigma_k^2(t) = D_k/b_k + [\sigma_k^2(0) - D_k/b_k]\exp(-2b_k t), \quad (6)$$

where $\bar{x}_k(t)$ is the mean of the concentration distribution and $\sigma_k^2(t)$, its variance about the mean. Also, equating $\partial C_k(x, t)/\partial t$ and the net flows in eqs. (1) to zero and integrating analytically shows that the equilibrium isoelectric focusing pattern ($t = \infty$) consists of two gaussian peaks centered at a_k/b_k (i.e., pI_k) with variance D_k/b_k.

2.2. Simple isomerization, reaction (II)

The calculations are for the case in which $\mathcal{N}$ has the higher pI so that the equilibrium constant $K = \hat{C}_1(j, t_n)/\hat{C}_2(j, t_n)$. ($\hat{}$ denotes chemical equilibrium.) Independent transport of $\mathcal{M}$ and $\mathcal{N}$ over Δt is calculated as described above. After each time cycle a new value of the constituent concentration, $\bar{C}(j, t_{n+1})$, is computed from the concentrations of the two species as changed by transport,

$$\bar{C}(j, t_{n+1}) = \bar{C}_1(j, t_{n+1}) + \bar{C}_2(j, t_{n+1}) \quad (7)$$

and chemical equilibrium is recalculated by imposing the mass action and conservation expressions

$$\hat{C}_2(j, t_{n+1}) = (1 + K)^{-1}\bar{C}(j, t_{n+1}), \quad (8)$$

$$\hat{C}_1(j, t_{n+1}) = \bar{C}(j, t_{n+1}) - \hat{C}_2(j, t_{n+1}). \quad (9)$$

These new values of the concentration serve us the starting distribution of material for the next time cycle of transport followed by chemical recquilibration, and so on.

Error estimates are provided by equations analogous to eqs. (5) and (6) in which the subscript k is dropped,

and D, a and b are replaced by their average values,

$$\bar{u} = (Ku_1 + u_2)(1 + K)^{-1} . \quad (10)$$

It can be shown analytically that the equilibrium isoelectric focusing pattern consists of a single gaussian peak centered at $\bar{a}/\bar{b}$ [pI, averaged according to eq. (10) if $b_1 = b_2$] with variance $\bar{D}/\bar{b}$.

2.3. Ampholyte-induced isomerization, reaction (I)

For the case in which $\mathcal{MA}_n$ has the higher pI, the calculation of transient isoelectric focusing patterns is the same as described above for simple isomerization except that the equilibrium constant is defined in each segment to be

$$K = \hat{C}_1(j, t_n)/\hat{C}_2(j, t_n)[\bar{C}_{\mathcal{A}}(j)]^n , \quad (11)$$

where $\bar{C}_{\mathcal{A}}(j)$ is the time-invariant, average constituent concentration of ampholyte* in segment j. Thus, one merely replaces the equilibrium constant in eq. (8) by the apparent equilibrium constant $K'(j) = K[\bar{C}_{\mathcal{A}}(j)]^n$. A gaussian distribution of constituent ampholyte (in one case a sum of such distributions) is assumed,

$$C_{\mathcal{A}}(x) = C_{\mathcal{A},\max} \exp\{-\tfrac{1}{2}[(x - \bar{x})/\sigma]^2\} \quad (12)$$

and

$$\bar{C}_{\mathcal{A}}(j) = (1/\Delta x) \int_{x_{j-1}}^{x_j} C_{\mathcal{A}}(x)\,dx . \quad (13)$$

In all the calculations $K'(I) = \hat{C}_1(I, t_n)/\hat{C}_2(I, t_n) \equiv 1$, where I is the segment in which the inflection point of the ampholyte distribution is located; i.e., $x_I - \Delta x/2 = \bar{x} \pm \sigma$.

To calculate the equilibrium isoelectric focusing pattern we note that the continuity equation for constituent macromolecule is

$$\frac{\partial \bar{C}(x,t)}{\partial t} = \frac{\partial}{\partial x}\left[\bar{D}(x,t)\frac{\partial \bar{C}(x,t)}{\partial x} - \bar{V}(x)\bar{C}(x,t)\right] , \quad (14)$$

in which

$$\bar{D}(x,t) = \frac{D_1K'(x) + D_2}{1 + K'(x)} + \frac{D_1 - D_2}{[1 + K'(x)]^2}\frac{dK'(x)}{dx}\left[\frac{\partial \ln \bar{C}(x,t)}{\partial x}\right]^{-1} ,$$

$$\bar{V}(x) = [V_1(x)K'(x) + V_2(x)][1 + K'(x)]^{-1} , \quad K'(x) = K[C_{\mathcal{A}}(x)]^n . \quad (15)$$

Equating $\partial \bar{C}(x,t)/\partial t$ to zero, noting the physical requirement that $(\bar{D}d\bar{C}/dx - \bar{V}\bar{C}) = 0$ at equilibrium, and integrating with respect to x for a column 1.5 cm long gives the equilibrium distribution

$$\bar{C}(x) = \frac{\int_0^{1.5} \bar{C}(z)\,dz}{\int_0^{1.5} \exp[\int_{x_a}^{z} \lambda(y)\,dy]\,dz} \exp\left[\int_{x_a}^{x} \lambda(y)\,dy\right] \quad (16)$$

$$\lambda(y) = \frac{V_1(y)K'(y) + V_2(y)}{D_1K'(y) + D_2} - \frac{(D_1 - D_2)\,dK'(y)/dy}{[D_1K'(y) + D_2][1 + K'(y)]} , \quad (17)$$

in which $0 \leqslant x_a \leqslant 1.5$, and $A\int_0^{1.5} \bar{C}(z)\,dz$ is the total moles of macromolecule in the column of uniform cross-sectional area, A. To evaluate the integrals the column was divided into 99 equal intervals, and a four-point Gauss–Legendre quadrature formula applied over each interval [16]. The maximum relative error in the numerical approximation was about 10^{-7} as judged by comparison with calculations using a six-point quadrature formula.

This formulation is for $\mathcal{MA}_n$ having the higher pI. It also holds for $\mathcal{MA}_n$ having the lower pI, provided that the subscripts 1 and 2 are interchanged in eqs. (8)–(11) and (15)–(17).

Computations were made on the University of Colorado's CDC 6400 electronic computer. For the transport part of the calculations $\Delta t = 5$ s and $\Delta x = 0.005$ cm which satisfy the stability criterion employed previously [17]. Unless stated otherwise, the several parameters were assigned the values: $D_1 = D_2 = 3 \times 10^{-7}$ cm^2 s^{-1} for the noninteracting system and simple isomerization; diffusion coefficients for $\mathcal{M}$ and $\mathcal{MA}_n$, 3.6×10^{-7} cm^2 s^{-1} and 2.6×10^{-7} cm^2 s^{-1}, respectively; $\alpha = 6.75125$ pH units and $\beta = 0.5$ pH units cm^{-1}; pH dependence of μ arbitrarily taken similar to the hemoglobins in free solution with $E = 10$ V cm^{-1} determining the velocity gradients.

* Constituent ampholyte consists of zwitterionic, anionic and cationic forms of the molecule. It is assumed that all forms bind equally well to the macromolecule.

These conditions give velocity gradients of the order of magnitude often used in practice: $a_1 = 9.975 \times 10^{-5}$ cm s^{-1}, $a_2 = 4.975 \times 10^{-5}$ cm s^{-1} and $b_1 = b_2 = 1 \times 10^{-4}$ s^{-1} corresponding to $pI_1 = 7.25$ located at $x = 0.9975$ cm in a column 1.5 cm long, $pI_2 = 7.00$ at $x = 0.4975$ cm; x_I midway between the positions of pI's. Material balance was excellent (to better than 10^{-6}%) except in one instance where by design some macromolecule was allowed to escape from the cathodic end of the column, which acted as a sink for about 11% of the material. Computed isoelectric focusing patterns are displayed as plots of constituent concentration of macromolecule, $C \equiv \bar{C}$, against position, x; the overbars are also dropped when $\bar{C}_1$ and $\bar{C}_2$ are plotted.

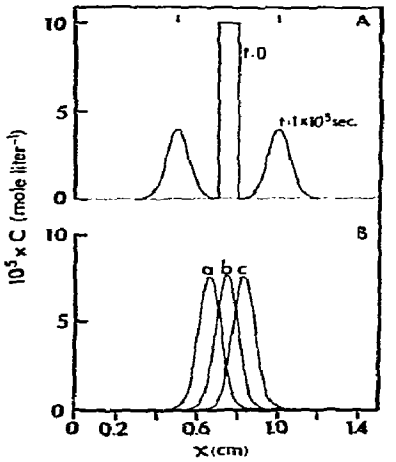

Fig. 1. Control calculation of isoelectric focusing patterns. A – Mixture containing equal proportions of two noninteracting macromolecules. B – Simple macromolecular isomerization [reaction (II)]: a, $K = 0.5$; b, 1.0; c, 2.0; $t = 1 \times 10^5$ s; same initial zone as in fig. 1B but with system at chemical equilibrium. Velocity gradients are the same as shown in fig. 2B; vertical arrows in this and following figures indicate positions of pI's.

3. Results

The control calculations displayed in fig. 1 serve a two-fold purpose: They allow assessment, through comparison with analytical relationships, of the accuracy of numerical simulation of transport in an electrofocusing column both in the absence and presence of macromolecular interaction; and they provide a framework within which to consider ampholyte-induced interactions. After 1×10^5 s of electromigration of two noninteracting macromolecules (fig. 1A) the distribution of material had for all practical purposes reached equilibrium, the isoelectric focusing pattern showing two virtually gaussian peaks centered at the pI's with variances agreeing to 0.2% with analytical prediction. The time-course of approach to equilibrium followed eqs. (5) and (6) with maximum deviations of $\approx 10^{-6}$% and 1.2%, respectively. The pattern for simple isomerization (fig. 1B) shows a single gaussian peak focused at $\overline{pI}$ determined by the value of K, with essentially the same agreement between numerical simulation and analytical predictions.

Most of the calculations for ampholyte-induced isomerization [reaction (I)] assume either specific binding of one of the several carrier ampholytes that may be positioned in the region of the pI's of the isomers or nonspecific binding of all of the ampholytes of which one (or a closely spaced family with gaussian envelope) overwhelmingly dominates the region. Both broad and sharp distributions of ampholyte (fig. 2A), corresponding roughly to the extreme widths of the discrete,

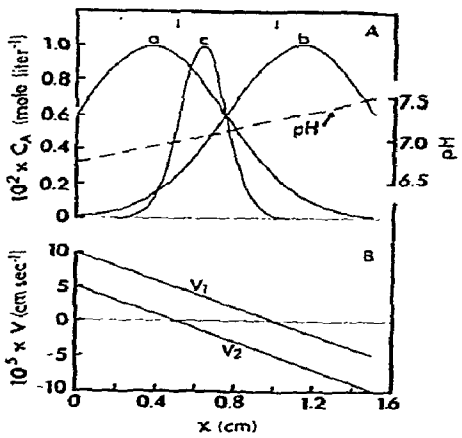

Fig. 2. Parameters of the calculations for ampholyte-induced isomerization [reaction (I)]. A – Environment created by the steady state distribution of carrier ampholytes: a, broad distribution ($\sigma = 0.373$ cm) of ampholyte used to calculate the isoelectric focusing patterns presented in figs. 3, 4 (patterns a and b), and 5; b, broad distribution pertaining to pattern c in fig. 4; c, sharp distribution ($\sigma = 0.118$ cm) pertaining to figs. 6–8. B – Velocity gradients of macromolecular species pertaining to figs. 3–8.

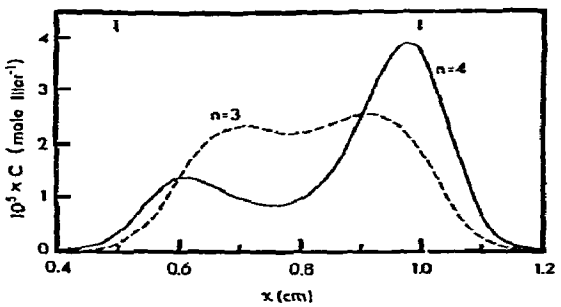

Fig. 3. Theoretical equilibrium isoelectric focusing patterns for ampholyte-induced macromolecular isomerization [reaction (I)]: pI of $\mathcal{NA}_n$ lower than $\mathcal{M}$; ampholyte distribution, curve a in fig. 2A; $K = (6.04 \times 10^{-3})^{-n}$ M^{-n}.

steady-state zones of "Ampholines" visualized experimentally [18], have been examined. Let us first consider the broad distribution whose cathodic flank traverses the region of interest (curve a in fig. 2A). Two cases can be discerned depending upon the relative pI's of $\mathcal{M}$ and $\mathcal{NA}_n$.

Case 1. As illustrated in fig. 3, when the pI of $\mathcal{NA}_n$ is lower than $\mathcal{M}$, the equilibrium isoelectric focusing pattern is bimodal for $n \geq 3$, although the peaks are not positioned at the two pI's. This is in contrast to the unimodal patterns shown by simple isomerization (fig. 1B) and reminiscent of what one would expect for a mixture of two noninteracting macromolecules with overlap of the focused peaks. Resolution of the pattern into two peaks when isomerization is induced by binding of ampholyte can be understood in terms of a dynamic equilibrium situation, in which the sense of the steady-state distribution of ampholyte governs the local equilibrium composition of macromolecule along the isoelectric focusing column. Thus, mass action favors $\mathcal{NA}_n$ in the region of its pI where the concentration of ampholyte is high, while $\mathcal{M}$ is favored in the region of its pI where the concentration of ampholyte is relatively low. This principle acting in concert with transport of individual macromolecular species, toward their respective pI's for driven transport (net diffusional and driven transport of constituent macromolecular being zero), prescribes a higher concentration near the ends of the pattern than in the middle. In other words, the two peaks correspond to different equilibrium compositions each enriched in the isomer of proximal pI (look ahead to fig. 5B), and not to separated isomers.

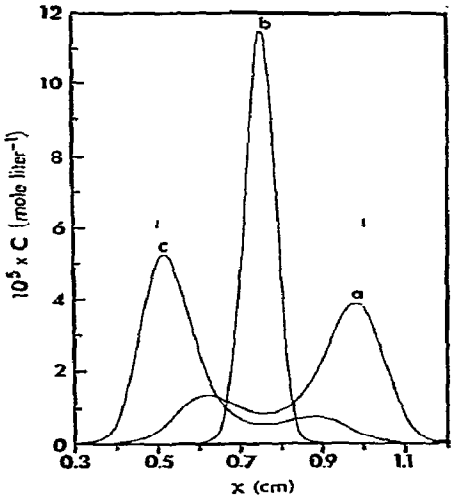

Fig. 4. Equilibrium isoelectric focusing patterns for ampholyte-induced isomerization [reaction (I) with $n = 4$ and $K = 7.50 \times 10^8$ M^{-4} in this and the following figures]: a, pI of $\mathcal{NA}_n$ lower than $\mathcal{M}$, ampholyte distribution given by curve a in fig. 2A; b, pI of $\mathcal{NA}_n$ higher than $\mathcal{M}$, ampholyte distribution given by curve a in fig. 2A; c, pI of $\mathcal{NA}_n$ higher than $\mathcal{M}$, ampholyte distribution given by curve b in fig. 2A.

Case 2. When the pI of $\mathcal{NA}_n$ is higher than $\mathcal{M}$, the pattern is unimodal (pattern b in fig. 4) with the peak sharply focused at the position where $K'(I) \equiv 1$. This is so because mass action favors $\mathcal{M}$ in the region of the pI of $\mathcal{NA}_n$ and vice versa, so that driven transport of either species toward its pI results in conversion to the other isomer which, in turn, is driven back toward the center of the pattern. Consistent with this explanation and that given for case 1, resolution into two peaks does occur (pattern c in fig. 4) when it is the anodic flank of the distribution of ampholyte which traverses the region of interest (curve b in fig. 2A).

The time-course of approach to the bimodal equilibrium distribution follows biphasic kinetics (fig. 5). During the first phase the transient isoelectric focusing pattern resolves into two peaks of about the same size at a relatively rapid rate controlled by electromigration of the two isomers (patterns a–d in fig. 5A). During the slower second phase, which is diffusion-dominated, one of the peaks grows at the expense of the other with minor shifts in the position-

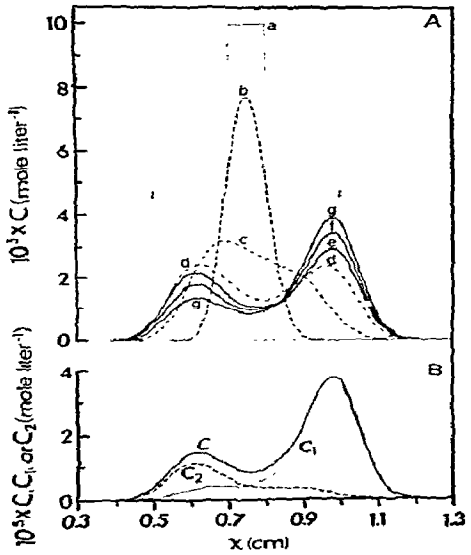

Fig. 5. Isoelectric focusing patterns for ampholyte-induced isomerization (pI of $\mathcal{NA}_n$ lower than $\mathcal{M}$; ampholyte distribution, curve a in fig. 2A). A – Time-course of approach to the equilibrium pattern: a, $t = 0$; b, transient pattern at $t = 2.5 \times 10^3$ s; c, 1.75×10^4 s; d, 5×10^4 s; e, 1×10^5 s; f, 2×10^5 s; g, equilibrium pattern. B – Transient pattern at 4×10^5 s showing concentration profiles of constituent macromolecule and individual species.

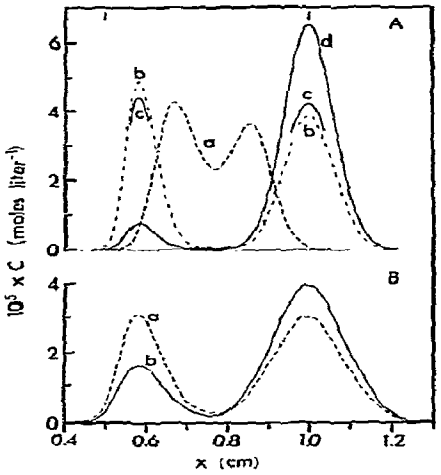

Fig. 6. Isoelectric focusing patterns for ampholyte-induced isomerization (pI of $\mathcal{NA}_n$ lower than $\mathcal{M}$; ampholyte distribution, curve c in fig. 2A; $t = 0$ as in fig. 5A). A – Time-course of approach to the equilibrium pattern: a, $t = 5 \times 10^3$ s; b, 2×10^5 s; c, 4×10^5 s; d, equilibrium pattern; similar results for $n = 2$. B – Increased rate of approach to equilibrium at halved velocity gradient ($a_1 = 4.9875 \times 10^{-5}$ cm s^{-1}, $a_2 = 2.4875 \times 10^{-5}$ cm s^{-1}, $b_1 = b_2 = 5 \times 10^{-5}$ s^{-1}): a, transient pattern at 2×10^5 s; b, equilibrium pattern.

ing of the extrema in the pattern (transient patterns d–f in fig. 5A and the transient pattern of fig. 5B, which is close to the equilibrium distribution given by pattern g in fig. 5A). This biphasic behavior is a consequence of two transient processes referred to as cooperative-uncoupling and field-uncoupling of the isomers. In cooperative-uncoupling the cooperativity of the reaction with respect to ampholyte and the gradient of ampholyte, both of which determine $K'(I)$, act to uncouple the system such that it effectively behaves like a mixture of two noninteracting macromolecules during the first kinetic phase, one of the peaks in the pattern being positioned close to the pI of $\mathcal{M}$. This effect is enhanced by field-uncoupling in which there is rapid separation of the two peaks by electromigration without opportunity for significant exchange of material via diffusion across the point x_I where the constituent velocity, $\bar{V}(I)$, is zero *. It is diffusion across x_I that is rate limiting in the second kinetic phase. In this connection we note that the minimum in the transient patterns remains cathodic to x_I until the equilibrium distribution is reached, thereby assuring that a finite gradient of macromolecule, upon which diffusional flow depends, exists at x_I throughout the approach to equilibrium.

The two uncoupling processes manifest themselves most vividly (fig. 6A) when the distribution of ampholyte is sharp (curve c in fig. 2A). Because of particularly effective cooperative-uncoupling occasioned by the steep gradient of ampholyte, field-uncoupling can act efficaciously to remove most of the material from the center of the pattern and, is so doing, to essentially minimize the gradient of macromolecule at x_I. Consequently, the second kinetic phase proceeds very slowly. Field-uncoupling can be relieved by decreasing the velocity gradients (by decreasing either the pH dependency of the mobilities or E) ** thus allowing increased

* There can be no field-uncoupling in the absence of cooperative-uncoupling as witnessed by simple isomerization (fig. 1B) whose transient isoelectric focusing patterns are strictly unimodal.

** Footnote: see next page.

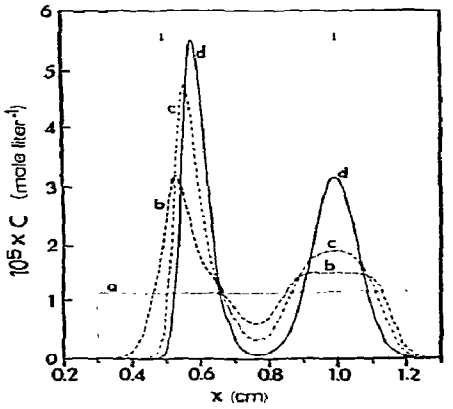

Fig. 7. First phase of the time-course of approach to isoelectric focusing equilibrium from an initially broad zone of macromolecule, conditions otherwise the same as in fig. 6A: a, $t = 0$; b, 2.5×10^3 s; c, 5×10^3 s; d, 1.5×10^4 s; equilibrium pattern given by pattern d in fig. 6A.

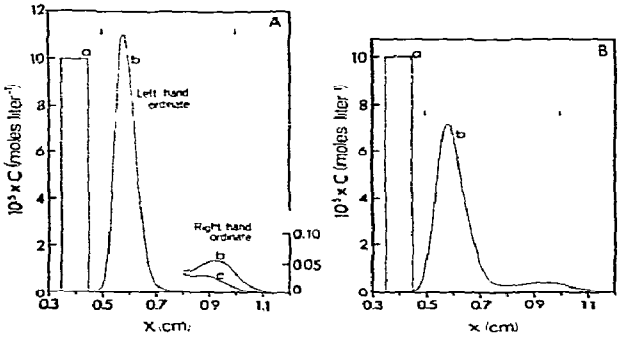

Fig. 8. First phase of the time-course of approach to isoelectric focusing equilibrium from an initially narrow zone of macromolecule positioned anodically to both pI's. A – Distribution of ampholyte and other parameters as in fig. 6A: a, $t = 0$; b, 4×10^4 s; c, 3×10^4 s; equilibrium pattern given by pattern d in fig. 6A. B – Effect of halving the velocity gradients, distribution of ampholyte and other parameters as in fig. 6B: a, $t = 0$, b, 8×10^4 s, which is the field-equivalent time of pattern b in fig. 8A; equilibrium pattern given by pattern b in fig. 6B.

diffusional flow across x_I at all stages, so that the equilibrium distribution is approached much more rapidly (fig. 6B).

These results are for a narrow initial zone of macromolecule centered between the pI's. While the equilibrium isoelectric focusing pattern is independent of initial conditions given the same total amount of material in the column, the time-course of approach to equilibrium is dependent upon initial conditions. When the macromolecule is distributed initially in a broad zone encompassing both pI's (fig. 7), the first kinetic phase of approach to equilibrium is characterized by one peak migrating inwards from the anodic end of the column toward its final position in the isoelectric focusing pattern, with simultaneous formation of the second peak from material migrating inwards from the cathodic end and outwards from the region between the pI's. A rather different picture is seen when a narrow initial zone is positioned either anodically or cathodically to both pI's. As illustrated in fig. 8A, a major peak positions itself just internally to the proximal pI, while a second peak grows very slowly in the vicinity of the distal pI at the expense of the first one. The slow growth of the second peak is due predominantly to cooperative-uncoupling, with field-uncoupling acting to sharpen the major peak to the point where the gradient of macromolecule at x_I almost vanishes. The latter effect can be partially relieved by decreasing the velocity gradient (fig. 8B).

So far we have confined our attention to the region of the isoelectric focusing column in the immediate vicinity of the pI's. We now turn to a different aspect of isoelectric focusing; namely, migration of the zone of macromolecule down the column enroute to its isoelectric region. Of interest here is possible interaction of the macromolecule with carrier ampholytes positioned along the route. Conceivably, such interaction could involve either a specific ampholyte or all of the ampholytes in accordance with reaction (I). The continuously changing profile of the zone as affected by interaction with a specific ampholyte is shown in fig. 9: As the zone rides up the anodic flank of the ampholyte distribution it sharpens considerably more than one would expect from the intrinsic velocity

** In the actual calculation the pH dependency of the mobilities was decreased. Another way of viewing the formulation is that E was decreased holding both the pH dependency of the mobilities and the variance of the ampholyte distribution constant; conceptual failure to relax the ampholyte distribution would not negate the conclusion reached, since relaxation acts to enhance the effect of decreasing the velocity gradients. In any case, the calculation demonstrates the principle involved. Also, it is clear that, in practice, the shape of the transient and equilibrium isoelectric focusing patterns will be rather sensitive to E

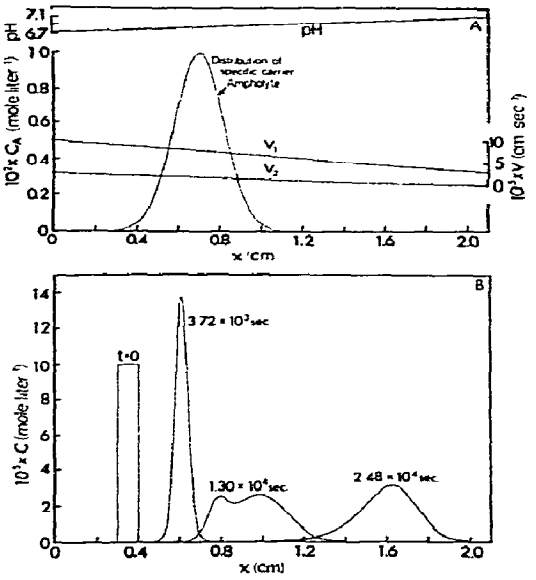

Fig. 9. Effect of interaction with a specific carrier ampholyte upon the shape of a zone of macromolecule migrating down an isoelectric focusing column enroute to its isoelectric region. A – Environment created by the steady state distribution of carrier ampholytes: $a_1 = 9.9883 \times 10^{-5}$ cm s^{-1}, $a_2 = 2.4958 \times 10^{-5}$ cm s^{-1}, $b_1 = 3.3333 \times 10^{-5}$ s^{-1}, $b_2 = 1.1905 \times 10^{-5}$ s^{-1}; specific ampholyte, $\sigma = 0.118$ cm. B – Transient profiles of macromolecule concentration.

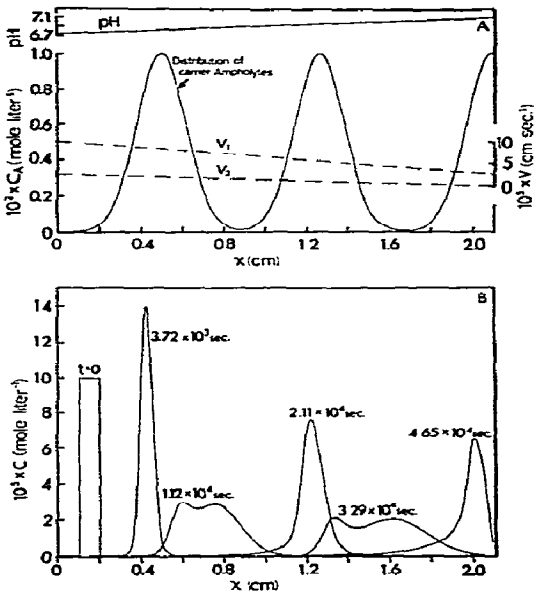

Fig. 10. Effect of interaction with all carrier ampholytes upon the shape of a zone of macromolecule migrating down an isoelectric focusing column enroute to its isoelectric region. A – Environment created by the steady state distribution of carrier ampholytes. velocity parameters and σ of individual ampholytes as in fig. 9A. B – Transient profiles of macromolecule concentration.

gradients per se, because $\mathcal{M}$ is converted by mass action into the slower migrating isomer $\mathcal{NA}_n$. Since $\mathcal{NA}_n$ lags $\mathcal{M}$, the leading edge of the zone moves considerably more slowly than its trailing edge, thus the hypersharpening without opportunity for resolution. Upon descending the cathodic flank of the distribution $\mathcal{NA}_n$ is continuously converted back to the faster migrating $\mathcal{M}$, and the hypersharpened zone now broadens and resolves into two peaks under the influence of cooperative- and field-uncoupling of the isomers. Resolution is transient, however, because once the ampholyte is left behind all of the macromolecule is in the form $\mathcal{M}$; as cooperative-uncoupling plays out its role, field-uncoupling abrogates resolution. The resulting unimodal zone then resharpens as it continues to migrate down the column, because intrinsically its trailing edge moves more rapidly than its leading edge. Essentially the same explanation applies when the interaction is with all of the ampholytes positioned along the route of migration. As shown in fig. 10, the zone of macromolecule successively hypersharpens and resolves into two peaks each time it crosses one of the peaks in the distribution of ampholytes.

4. Discussion

The foregoing results demonstrate that a single protein or other amphoteric macromolecule can give isoelectric focusing patterns showing two peaks due to reversible binding of carrier ampholyte with accompanying macromolecular isomerization. This is so despite rapid chemical equilibration. Moreover, ampholyte-induced association–dissociation reactions (Cann et al., work in progress) and pH-dependent conformational transitions [19] behave similarly. This is of considerable practical importance since the bimodal patterns exhibited by interacting systems could easily be misinterpreted as indicative of inherent heterogeneity with respect to isoelectric point. One

means of detecting interaction is to focus the sample from different points of insertion into the column (compare figs. 6A, 7 and 8A), but unequivocal proof of heterogeneity is afforded only by fractionation. In the fractionation test the protein in each peak is isolated. The resulting fractions are reconstituted to the concentration of the unfractionated material (a precautionary procedure which takes cognizance of possible macromolecular association–dissociation) and resubjected to isoelectric focusing. For interaction each fraction will behave like the unfractionated material and show two peaks, while for heterogeneity a single focused peak will be obtained. The investigation of Talbot [9] on the pH-dependent conformational states of the 12S subunit protein of foot-and-mouth disease virus is exemplary. In these experiments the forementioned procedural variations were combined systematically with fractionation in such a way as to leave no doubt as to the interacting nature of the system.

A corollary pertaining to the routine determination of isoelectric points is that the sample should always be focused from different points of insertion into the column. If, for example, an interacting system were to be focused only from a point anodic (or cathodic) to its isoelectric region, the interaction might well escape attention (fig. 8A); and the apparent isoelectric point of the presumed noninteracting protein would be in error, perhaps, by as much as ±1.5 pH units (fig. 21.1 in ref. [9]).

The results of the theoretical calculations also furnish possible explanations for hitherto puzzling experimental observations. For example [12], both α-glycerol phosphate dehydrogenase and pyruvate kinase, when focused from an initially uniform distribution throughout a density-gradient isoelectric focusing column, give transient patterns showing two peaks migrating from either end of the column. As the two peaks approach the isoelectric region they either coalesce into a single peak or, possibly, one of the peaks grows at expense of the other as judged from the few transient patterns presented. Clearly, the described behavior is indicative of an "Ampholine" – or pH-induced change in protein conformation or state of association. In another vein, Catsimpoolas [10] has observed a moving zone of protein split into two zones and, after a time, become one again during migration down a density-gradient column enroute to its isoelectric pH. Mayers [11] reports a more complex behavior for DNT insulin on a gel column: Not only does the moving zone split into two which then coalesce into one but it does so repeatedly during passage down the column. The calculations presented in figs. 9 and 10 furnish an explanation of these observations in terms of interaction with a specific "Ampholine" in the first instance, and with all of the "Ampholines" positioned along the column in the second.

Finally, the new insights provided by these calculations add to the store of fundamental understanding required for the application of isoelectric focusing to the detection and characterization of a variety of biochemical reactions such as the interaction of enzymes with inhibitors and allosteric affectors and the interaction of macromolecules with each other. The peculiar sensitivity of isoelectric focusing might permit detection of subtle, ligand-induced conformational changes which are beyond the reach of other methods. Recently, Drysdale [20] reviewed preliminary findings which indicate that isoelectric focusing holds promise for the study of these several classes of interaction.

References

[1] H. Svensson, Acta Chem. Scand. 15 (1961) 325.
[2] H. Svensson, Acta Chem. Scand. 16 (1962) 456.
[3] O. Vesterberg and H. Svensson, Acta Chem. Scand. 20 (1966) 820.
[4] O. Vesterberg, Acta Chem. Scand. 23 (1969) 2653.
[5] H. Haglund, Methods Biochem. Anal. 19 (1971) 1.
[6] N. Catsimpoolas, Ann. NY Acad. Sci. 209 (1973) 1–529.
[7] P.G. Righetti and J.W. Drysdale, J. Chromatog. 98 (1974) 271.
[8] J.W. Drysdale and P. Righetti, Biochemistry 11 (1972) 4044.
[9] P. Talbot, in: Isoelectric focusing, eds. J.P. Arbuthnott and J.A. Beeley (Butterworths, London, 1975) p. 270.
[10] N. Catsimpoolas, Ann. NY Acad. Sci. 209 (1973) Discussion p. 63.
[11] Mayers, Ann. NY Acad. Sci. 209 (1973) Discussion p. 63.
[12] J.N. Behnke, S.M. Dagher, T.H. Massey and W.C. Deal Jr., Anal. Biochem. 69 (1975) 1.
[13] W.B. Goad, in: Interacting macromolecules. The theory and practice of their electrophoresis, ultracentrifugation, and chromatography, ed. J.R. Cann (Academic Press, New York, 1970) ch. 5.
[14] W.B. Goad and J.R. Cann, Ann. NY. Acad. Sci. 164 (1969) 172.

[15] J.R. Cann and G. Kegeles, Biochemistry 13 (1974) 1868.
[16] B. Carnahan, H.A. Luther and J.O. Wilkes, Applied numerical methods (Wiley, New York, 1969) pp. 101–112.
[17] J.R. Cann and W.B. Goad, J. Biol. Chem. 240 (1965) 148.
[18] K. Felgenhauer and S.J. Pak, Ann. NY Acad. Sci. 209 (1973) 147.
[19] D.I. Stimpson and J.R. Cann, Biophys. Chem. 7 (1977) 115.
[20] J.W. Drysdale, in: Methods of protein separation, Vol. 1, ed. N. Catsimpoolas (Plenum Press, New York, 1975) ch. 4.